Structural correlations in $La_{0.7}Pb_{0.3}(Mn_{1-x}Fe_x)O_3$ manganites as probed by small-angle and polarized neutron diffraction

2006 J. Phys.: Condens. Matter 18 9951

(http://iopscience.iop.org/0953-8984/18/43/017)

INSTITUTE OF PHYSICS PUBLISHING JOURNAL OF PHYSICS: CONDENSED MATTER

J. Phys.: Condens. Matter **18** (2006) 9951–9966 doi:10.1088/0953-8984/18/43/017

Structural correlations in $La_{0.7}Pb_{0.3}(Mn_{1-x}Fe_x)O_3$ manganites as probed by small-angle and polarized neutron diffraction

J Gutierrez[1,2], F J Bermejo[1,2], N Veglio[1,2], J M Barandiarán[1,2], P Romano[3], C Mondelli[4], M A González[5] and A P Murani[5]

[1] CSIC—Department of Electricity and Electronics, University Basque Country, PO Box 644, Bilbao 48080, Spain
[2] Consejo Superior de Investigaciones Científicas, Serrano 123, E-28006 Madrid, Spain
[3] ISIS Facility, Rutherford Appleton Laboratory, Chilton, Didcot, Oxon OX11 0QX, UK
[4] CNR-INFM and CRS Soft, Institut Laue Langevin 6, Rue Jules Horowitz, F-38042 Grenoble Cedex 9, France
[5] Institut Laue Langevin, BP 156x, F-38042 Grenoble Cedex 9, France

E-mail: jon@we.lc.ehu.es (J Gutierrez)

Received 20 June 2006, in final form 22 September 2006
Published 13 October 2006
Online at stacks.iop.org/JPhysCM/18/9951

Abstract

Small-to-medium-angle neutron diffraction as well as a full neutron polarization study of CMR manganites of general formula $La_{0.7}Pb_{0.3}(Mn_{1-x}Fe_x)O_3$, from $x = 0$ up to $x = 0.2$, reveal the presence of nanometre-sized magnetic domains having characteristic dimensions about one order of magnitude smaller than the crystal grain sizes. The role played by such entities as main drivers of the magnetic ordering transition is established here by analysis of the diffraction data. The model employed is then validated from data derived from polarized neutron diffraction. The latter also provides a direct insight into the presence of antiferromagnetic regions that arise as a consequence of competing interactions brought about by Fe substitution on the Mn site. The results are finally discussed within the context of recent findings on related materials.

(Some figures in this article are in colour only in the electronic version)

1. Introduction

A formidable amount of work has been devoted aiming towards the understanding of the structure and properties of colossal magnetoresistive (CMR) manganites [1]. These materials are sensitive to small changes in external conditions as well as in composition and show rather complex phase diagrams. While the CMR effect has been reported for a good number of materials, its very origin still remains a widely debated issue [2–5]. Nowadays it seems well established that the double exchange (DE) mechanism [6] cannot by itself account for the

observed effects. Other mechanisms involving electron–phonon coupling [7], electron–magnon interactions [5], phase- and charge-segregation [4, 8] or some other electronic effects [9] have been proposed to explain the variety of observed phenomena, although the respective merits of each mechanism remain a matter of debate.

The complicated phenomena exhibited by these materials is evidenced by the change of their properties upon increasing hole doping. The parent compound for one of the best studied families, $LaMnO_3$, has an antiferromagnetic (AF) structure below $T_N = 140$ K consisting of stacked planes along the crystallographic c-direction which results from an orbital-ordered state [10] achieved at 750 K. Magnetic coupling between the Mn^{3+} ions is mediated by super-exchange interactions. Increasing hole doping by cationic species $La_{1-x}M_x$ (M = Ca, Ba, Sr, Pb or other divalent cations) translates into dramatic effects on both structure and transport properties. This results from the creation of mobile Mn^{4+} species on the Mn sites having as a net effect the possibility for e_g electrons to hop depending upon the configuration of neighbouring spins. At low cation doping the material, as expected from mean-field arguments [6], shows a canted AF structure which in addition is known to be magnetically inhomogeneous [11]. Larger doping ratios give rise to ferromagnetism as the well-studied case of $La_{0.7}Pb_{0.3}MnO_3$ clearly shows. In addition, hole doping with Sr [1] or Pb [12] is of practical interest since it leads to high magnetic ordering temperatures (350 K for $La_{0.7}Pb_{0.3}MnO_3$) as well as to fully stable ferromagnetic (FM) character. This contrasts with the effects brought forward by Ca substitution which results in the introduction of an FM instability as well as in lower ordering temperatures (265 K for $La_{0.7}Ca_{0.3}MnO_3$) [13]. Such a difference in behaviour is understood on the basis of the larger ionic radius of Pb versus Ca ($\langle r_{Pb}\rangle = 1.49$ Å, $\langle r_{Ca}\rangle = 1.34$ Å) [14]). Here we choose hole doping using Pb which provides a large average radius for the La-hole site.

As is known since the systematic studies carried out by Searle *et al* [12], the static magnetization for $La_{1-x}Pb_xMnO_3$ ($0.25 < x < 0.45$), while showing features much akin to those for ferromagnets, displays Brillouin functions that decrease more rapidly than expected. Strikingly enough, the spin-wave spectrum as well as the Curie temperature ($T_C = 350$ K) for the metallic ferromagnet $La_{0.7}Pb_{0.3}MnO_3$ can be reasonably well accounted for in terms of a simple cubic Heisenberg Hamiltonian with a sole nearest-neighbour coupling of 8.8 meV [15]. However, and contrary to the well-studied cases on insulating ferromagnets, the high-frequency spin waves were strongly damped with increasing temperature [15], even if the accompanying changes in ferromagnetic order were rather small. In fact, and in common with findings for two Ca-substituted compounds, the temperature evolution of the intensities of high-energy magnetic excitations are found to deviate from Bose statistics in a way akin to that expected for magnetic quantum levels in super-paramagnetic spin clusters [16].

Here we extend our investigations into aspects pertaining to the structure of $La_{0.7}Pb_{0.3}MnO_3$ and some related compounds at the nanoscale. A previous communication dealt with the intrinsic inhomogeneity inherent to one of these materials [17], which was quantified by means of a model of a liquid composed by magnetic droplets. The main conclusion was the existence of ferromagnetic clusters well above the magnetic transition temperature having their magnetic moments randomly oriented. These magnetic droplets react quickly to the presence of magnetic fields or to lowering the temperature and remain as well-defined entities down into the ferromagnetic state, even if relatively long-ranged ferromagnetic regions are finally formed.

Doping $La_{0.7}Pb_{0.3}MnO_3$ with transition metals has some practical advantages concerning the macroscopic magnetization and magnetoresistance [20]. The Fe ions enter these samples as Fe^{3+} and, as demonstrated by field-dependent Mössbauer studies [21] on the Sr isomorph, the coupling between Fe and Mn is of antiferromagnetic nature. The Fe ions serve to fine

tune the double exchange (DE) mechanism by breakage of the DE chain, and its strength gets progressively reduced as the Fe concentration increases, up to a point where Fe doping leads to substantial frustration, and reaching a limit of $x = 0.20$ where a state of the spin system showing common characteristics with cluster spin glasses (CSGs) is achieved [18, 19]. On the other hand, the close ionic radii of Fe^{3+} and Mn^{3+} [22] makes such replacement yield a rather small lattice distortion.

Here we aim to provide a better understanding of the underlying phenomenology exhibited by CMR manganites by means of a structural study on a series of $La_{0.7}Pb_{0.3}(Mn_{1-x}Fe_x)O_3$ manganites, where the Fe content is varied from the $x = 0$ FM state up to $x = 0.2$. The mechanism by which Fe alters the electronic properties of manganites comes from the completely filled Fe e_g band, hampering any transition between Mn^{3+} and Fe^{3+}. As a result, replacing Mn^{3+} with Fe^{3+} leads to a concomitant decrease of the ratio Mn^{3+}/Mn^{4+} which depletes the number of possible hopping sites. This alters the DE ferromagnetic exchange mechanism as well as the characteristic metallic properties.

Our previous study [17] has reported on the emergence of relatively large inhomogeneities of magnetic origin as detected on $La_{0.7}Pb_{0.3}(Mn_{0.9}Fe_{0.1})O_3$ by means of a systematic exploration of the small-to-medium-angle diffraction patterns comprising wavevectors within $0.02\ \text{Å}^{-1} \leqslant Q \leqslant 0.5\ \text{Å}^{-1}$. Here, we extend such a preliminary study concentrating upon the effect of Fe doping on the characteristic dimensions of such inhomogeneities as well as studying the purely magnetic single-differential cross-section which is carried out using full neutron polarization analysis on samples with increasing Fe content. In doing so we aim to establish the role of magnetic inhomogeneities in samples such as $La_{0.7}Pb_{0.3}MnO_3$ which in some respects behaves as a conventional ferromagnet up to those that are heavily doped which show neither spontaneous magnetization nor magnetic order beyond a scale of a few nanometres and show behaviour akin to those of cluster spin glasses.

2. Experimental details

Finely powdered samples of $La_{0.7}Pb_{0.3}(Mn_{1-x}Fe_x)O_3$, $0 \leqslant x \leqslant 0.2$, were synthesized by a sol–gel method described in [20]. This procedure yields homogeneous single-phase powders as shown by x-ray diffraction. Using transmission electron microscopy (TEM) the averaged grain sizes came out to be about 100 nm for the undoped composition, and ranging from 80 to 50 nm as the Fe content is increased. The temperature dependence of the magnetization $M_{DC}(T)$ was investigated by means of SQUID magnetometry [23, 20]. Zero-field-cooled–field-cooled (ZFC–FC) curves were measured at a field $H = 10$ mT. Hysteresis loops at 5 K and up to 7 T were also recorded. From the ZFC curves we have determined the Curie temperatures as those where the minimum in dM/dT is located. The results are shown in figure 1 and show both a decrease in magnetic ordering temperatures as the Fe doping increases and a noticeable broadening of the transition. The magnetic ordering temperatures are shown to decrease from 350 K for the parent compound down to 230, 160 and 95 K for $x = 0.1$, 0.15 and 0.2, respectively. This decrease in transition temperature is accompanied by a reduction of the low-temperature magnetic moment which yields for the saturated magnetization (i.e. as determined from Arrot plots) values per formula unit of 3.6, 2.9, 2.4 and 1 μ_B, respectively. With the exception of the sample with $x = 0.2$, the measured moments agree with those expected from $\mu = (1-x)\langle\mu\rangle_{Mn} - x\langle\mu\rangle_{Fe}$, that is, they are valid for a random substitution of Mn^{3+} by Fe^{3+} ions and antiferromagnetic coupling of these [24, 25], ($\langle\mu\rangle_{Fe} = 5\ \mu_B$).

To investigate the temperature dependence of magnetic correlations at micrometre to nanometre length scales through the ferromagnetic to paramagnetic (FM $\longrightarrow$ PM) transition

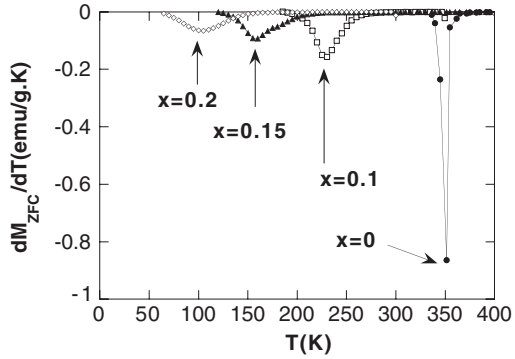

Figure 1. Determination of the magnetic ordering temperatures by means of temperature derivatives of the ZFC curves for the whole set of compounds.

we have carried out middle-to-small-angle neutron scattering (SANS) measurements using the instrument D16 at the Institute Laue Langevin (ILL, Grenoble, France). The neutron wavelength used in these experiments was $\lambda = 4.5$ Å, and the explorable range of momentum transfers was $0.02\ \text{Å}^{-1} \leqslant Q \leqslant 0.4\ \text{Å}^{-1}$. The instrument has a position-sensitive ^{3}He multidetector with 128×128 wires, with individual readout and distance between wires of 2 mm. The angular resolution achieved for the employed setup as measured using an external standard was 0.121°. The resolution function $R(\Omega)$ was then modelled using a Voigt profile.

The measured data from samples contained within a thin vanadium cylinder were collected using a single experimental setup. The measured counts after correcting for sample self-absorption, background and container scattering were transformed into single-differential cross-sections $\mathrm{d}\sigma/\mathrm{d}\Omega$ by means of normalization using a vanadium standard. To assess the importance of multiple scattering effects, the transmission factor was evaluated as

$$T = \exp -\phi \left[\frac{\lambda^2}{2\pi} \int_{Q_{\min}}^{Q_{\max}} \mathrm{d}Q\, Q\, \mathrm{d}\sigma/\mathrm{d}\Omega \right] \tag{1}$$

where ϕ stands for the sample diameter and the limits on the integral stand for the values given above. The obtained percentage value of 86.7% prompted the need for performing a multiple scattering correction. The correction procedures followed those implemented within the CORRECT code [26].

The analysis of the single-differential neutron scattering cross-sections followed steps delineated in a previous publication [17]. Briefly, the measured cross-section is decomposed as

$$\begin{aligned} \frac{\mathrm{d}\sigma}{\mathrm{d}\Omega} &= \left[\left.\frac{\mathrm{d}\sigma}{\mathrm{d}\Omega}\right|_s + \left.\frac{\mathrm{d}\sigma}{\mathrm{d}\Omega}\right|_m \right] \otimes R(\Omega) \\ \left.\frac{\mathrm{d}\sigma}{\mathrm{d}\Omega}\right|_s &= A_T S'_s(Q) P_s(Q) \\ \left.\frac{\mathrm{d}\sigma}{\mathrm{d}\Omega}\right|_m &= A_m P_m(Q) \left[S'_m(Q) + \left(\frac{B}{Q^2 + \left(\frac{1}{\xi}\right)^2} + \frac{C}{(Q^2 + \left(\frac{1}{\xi}\right)^2)^2} \right) \right], \end{aligned} \tag{2}$$

where the symbol $\otimes$ stands for convolution, and the subscripts s and m denote nuclear and magnetic contributions to the total cross-section. It is written in terms of scattering from ensembles of interacting spherical particles of structural (chemical) origin with a shape

determined by the form-factor P_s and interference (diffraction) effects accounted for by the $S'_s(Q)$ structure factor. In turn, the magnetic component comprises a term $S'_m(Q)$ to account for interference (diffraction) effects from an ensemble of magnetic particles and P_m represents the form factor (assumed to be spherical) including a polydispersity function represented by the Schultz distribution [29]. Finally, a Lorentzian (i.e., Ornstein–Zernike approximation supplemented by a squared-Lorentzian) term is here used on heuristic grounds in much the same way as those reported for several magnetic systems of rather different nature [27] to account for paramagnetic scattering. Such a combination significantly improves the data fitting, and the origin of the two terms is usually ascribed to fluctuations in the spin system as well as to scattering from static regions of spin ordering, respectively (see Hellman *et al* in [27]). The physical parameter entering such expression ξ that plays the role of a correlation length [28], paramagnetic fluctuations (see Birgeneau *et al* [27]).

The relevant parameters entering equation (2) for the ensuing discussions are those describing the particle form-factor and those entering the expression for the static structure factor $S(Q)$. In what follows we will circumscribe our attention into the three more physically significant parameters, namely the particle radii R, the correlation length for magnetic fluctuations $\xi(T)$ and the number density for magnetically interacting particles n. The interested reader is referred to our previous communication [17] for further details of the data analysis procedures.

To enable the separation of the purely magnetic signal from the spin-incoherent and the nuclear scattering (coherent plus incoherent), experiments using polarized neutron diffraction were carried out for all samples. For this purpose we used the D7 spectrometer hosted also at the ILL under the full (XYZ) polarization analysis mode [30, 31]. This instrument consists of three large Helmholtz coil pairs located outside the sample environment, allowing measurements to be performed with three orthogonal incident polarization directions, which enables the separation of all three spatial components as well as the ability to normalize them into an absolute scale.

Experiments were carried out using a wavelength of 4.8 Å, accessing a range of momentum transfers $0.2\ \text{Å}^{-1} \leqslant Q \leqslant 2.49\ \text{Å}^{-1}$, and temperatures spanning through the magnetic transition of each compound. The beam polarization was monitored upon sample cooling. Typical values for the flipping ratios as measured within the PM phase were about 24 for the X, Y and Z directions. However, the macroscopic ferromagnetism that develops below the ordering temperatures led to a reduction in flipping ratios down to values of about 3–5. These low values arise from substantial beam depolarization for all three components and preclude measurements well below the magnetic ordering transition.

As a criterion for choosing a temperature at which to carry out measurements, we chose the lowest temperature at which full polarization was maintained. While some previous exploratory measurements on some of the samples suggested that we could choose temperatures midway through the ordering transition, the actual results indicated that the explored magnetic correlations show a smooth dependence with temperature. In consequence, the measurements were performed at 370, 245, 180 and 120 K for the $x = 0$, 0.1, 0.15 and 0.2 samples, respectively.

3. Results

3.1. Structure at the nanoscale: unpolarized neutrons

An example of the temperature dependence of the neutron diffraction patterns for the parent compound $La_{0.7}Pb_{0.3}MnO_3$ in shown in figures 2 and 3. There we show, apart from the full

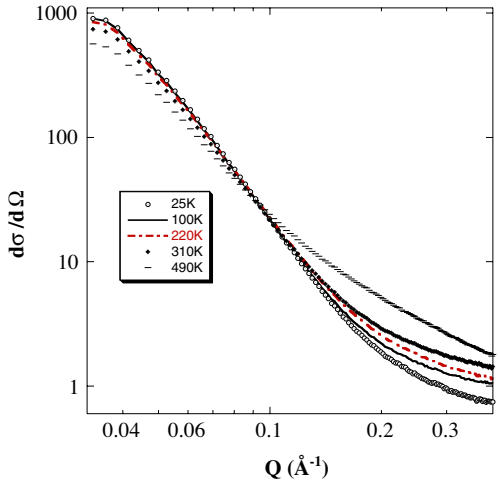

Figure 2. A set of diffraction patterns for the $La_{0.7}Pb_{0.3}MnO_3$ parent compound. Units are b/sr/formula unit.

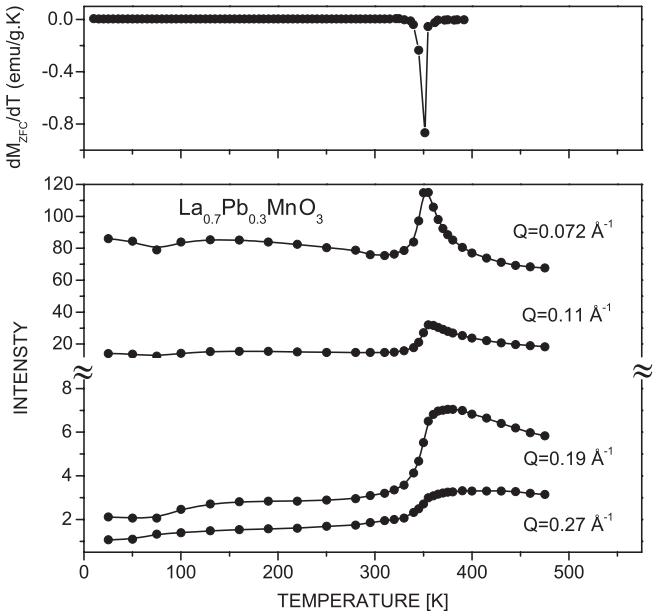

Figure 3. Temperature dependence of the diffraction intensities for $La_{0.7}Pb_{0.3}MnO_3$ corresponding to a set of selected momentum-transfers.

set of measured curves, the variation with temperature of the cross-sections at some selected values of the momentum-transfer. Figure 2 shows a pencil of curves with a clear crossover within the region of momentum-transfers of $0.04\ \text{Å}^{-1} \leqslant Q \leqslant 0.1\ \text{Å}^{-1}$. At the lowest explored temperature (25 K) and high Q-values, the curve shows a sigmoid shape having an intensity that goes well below that of the two curves measured above the Curie temperature (350 K). In contrast, the intensity for the lower wavevectors and the lowest temperature goes well above that corresponding to those above the ordering transition. The temperature dependence of

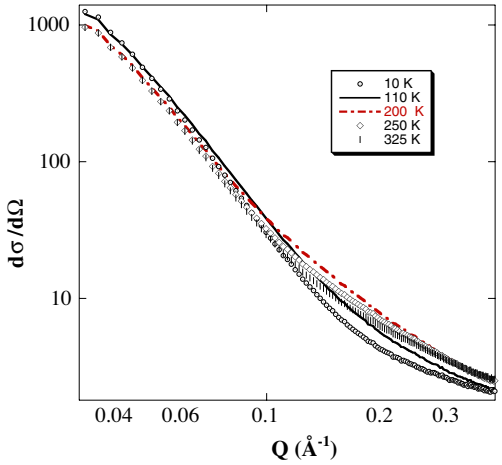

Figure 4. A set of diffraction patterns for the $La_{0.7}Pb_{0.3}Mn_{85}Fe_{0.15}MnO_3$ Fe-substituted compound. Units are b/sr/formula unit.

the diffracted intensity for a selected set of four Q-values is shown in figure 3. There we see that the shape of curves depicting the measured intensities transform from that showing relatively well-defined peaks at low Q to a stepwise decrease in intensity as the temperature is decreased through T_C for the higher wavevector. A glance at these data suggests that we are here witnessing a PM $\longrightarrow$ FM transition that is sampled by the lowest wavevectors, that is for length scales about $2\pi/Q \simeq 8$ nm and beyond, while the higher Q-values sample the onset of paramagnetic scattering above the ordering temperature. A direct comparison with macroscopic phenomena is provided by the temperature derivative of the ZFC curve drawn in the upper frame of the same figure. There we see how the macroscopic transition temperature matches that corresponding to the peak in intensities at low Q as well as the sharp step at higher momentum-transfers. In contrast, the PM $\longrightarrow$ FM transition appears as a far sharper feature in the macroscopic measurement than that sampled by neutron diffraction.

The data reported here show, on a model-independent basis, the presence of significant inhomogeneities giving rise to small-angle scattering of magnetic origin that exists even in the parent $La_{0.7}Pb_{0.3}MnO_3$ at temperatures well below magnetic ordering.

Data for the $x = 0.10$ composition have already been reported [17], and here we show for comparison purposes those concerning the $x = 0.15$ compound. The corresponding curves are shown in figures 4 and 5.

A comparison with the set of cross-sections shown in figure 4 shows that the variation with temperature of the scattering patterns is significantly less marked than that for the parent compound. The intensity versus temperature curves shown in figure 5 also depict far more sluggish features than those shown in figure 3. In fact, consideration of the two graphs just referred to together with that shown in figure 1 shows that the curves for the lowest wavevector mimic the behaviour of the temperature derivative of the macroscopic magnetization, showing a maximum at T_C and a width that becomes comparable to those of dM_{ZFC}/dT as $Q \longrightarrow 0$, while those for higher Q exhibit a more complex pattern.

A comparison of the diffraction patterns for the lowest wavevectors shows that the increase in height of the low-angle peak which displays a broad maximum centred at $Q \approx 0.025$ Å^{-1} upon crossing from above the magnetic ordering transition becomes less marked as the Fe content is increased. Such an increase is attributed to the enhancement of ferromagnetic

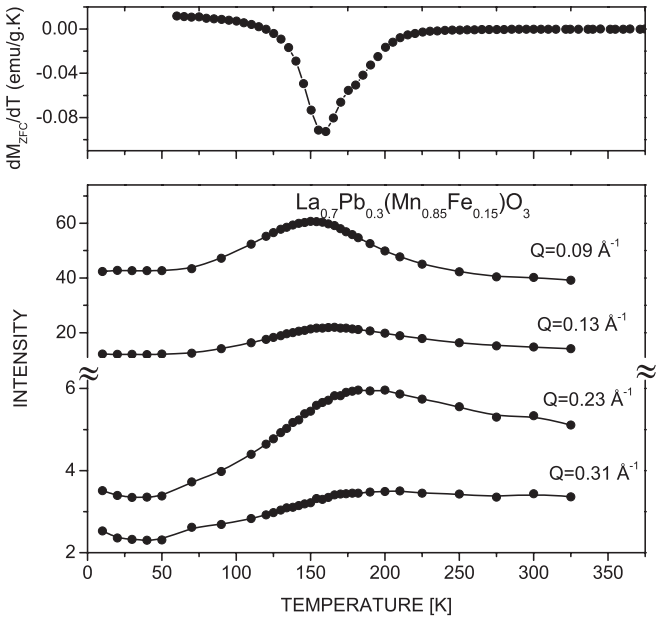

Figure 5. Temperature dependence of the diffraction intensities for $La_{0.7}Pb_{0.3}Mn_{85}Fe_{0.15}MnO_3$ corresponding to a set of selected momentum-transfers. The upper frame displays the temperature derivative of the ZFC curve and is drawn for comparison purposes.

interactions between nanoscopic magnetic entities upon crossing the transition. In real numbers this intensity is as much as 68% for $x = 0$ and 16% for $x = 0.1$, but it becomes barely detectable for $x = 0.20$.

As referred to above, the quantitative analysis of the diffraction patterns is carried out in terms of a model describing a set of interacting magnetic particles, assumed to be spherical having an average radius R_{av}, that give rise to a structure factor $S(Q)$ calculated within the Percus–Yevick (PY) approximation [17]. A summary of the relevant parameters is shown in figure 6.

The left-hand frame of figure 6 depicts the compositional dependence of the correlation length for magnetic fluctuations $\xi(T)$. There we see how the parent compound exhibits a narrow peak much like that expected for a ferromagnet across the ordering transition. The temperature of such a feature, 345 K $\pm$ 2.5 K, correlates well with the macroscopic T_C as determined by static magnetization measurements [23], and the same applies to all the Fe-doped compositions. The length scale for such fluctuations reaches some 20 nm, which is significantly smaller than the crystallite grain sizes of $\approx$100 nm as determined by TEM. Relatively small addition of the Fe dopant, that is 10%, has two measurable effects on this quantity. It reduces its maximum extent to approximately half that of the parent compound and also broadens the narrow peak shown by $La_{0.7}Pb_{0.3}MnO_3$ up to about 25 K. Higher Fe doping leads to further decrease in spatial extent of such fluctuations and also to further broadening of the shape of $\xi(T)$. Data for the two higher Fe compositions suggests that rather than a single transition taking place over a relatively well-defined range of temperatures, here we are dealing with superimposed transitions, in a way like that shown by recent AC susceptibility studies [19].

Data regarding the average particle radius R_{av} shown by the centre frames of figure 6 show two features worth remarking upon. The first concerns the rather small differences within the Fe-doped compounds that have values within the 34–40 Å range, while that concerning the

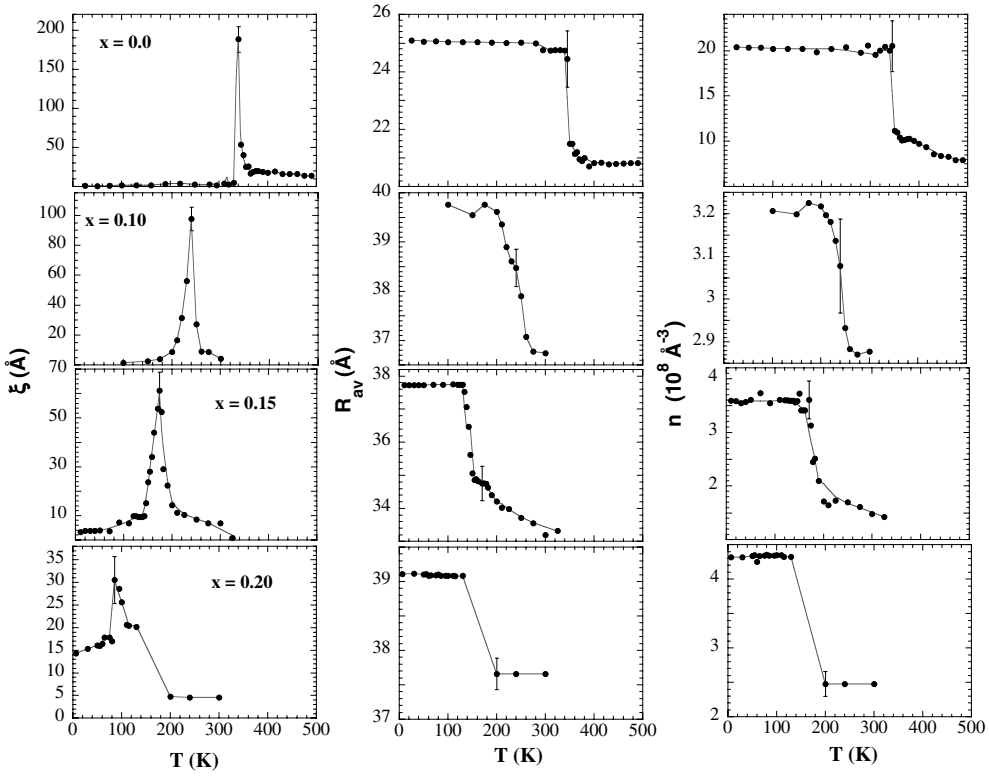

Figure 6. Relevant parameters resulting from the analysis of the diffraction intensities in terms of the model described in detail in [17]. Here ξ stands for a correlation length for critical (or paramagnetic) fluctuations, $R_{\rm av}$ is the average particle radius and n is the number density for magnetic particles. Notice that n specifies the packing fraction $\eta = \pi n\sigma^3/6$ where σ stands for the particle diameter. Values for other parameters such as the polydispersity factor were found not to significantly differ from those given in our previous communication [17]. Error bars depict the calculated largest error.

undoped sample yields values that are nearly one half of those. Second, the specific values for $R_{\rm av}$ do show a significant temperature dependence only within the range where the ordering transition takes place. In all cases a jump of about 10–15% in the magnitude of this quantity is registered when crossing the ordering transition.

Finally, perhaps the most remarkable result concerns the difference in magnetic particle number densities shown in the right-hand frame of figure 6. Such figures are to be compared with the average atomic number densities which vary from 1.70×10^{-2} Å^{-3} for $x = 0$ to 1.68×10^{-2} Å^{-3}, which result from the small but systematic expansion of the unit cell volume with increasing Fe content. Data shown in the right-hand side of figure 6 tell that the particle densities in the parent compound are close to an order of magnitude higher than those of the Fe-doped samples. The result correlates with the smaller particle size given by $R_{\rm av}$, and expressed in terms of the packing fraction η it amounts to a structure some 15% more highly packed for $La_{0.7}Pb_{0.3}MnO_3$ if compared to that for $x = 0.20$. The result can also be viewed in terms of the minimal distance between particles $d_{\rm min}$ that enters as a derived parameter in the PY model and amounts to a variation from about 16 nm in the parent sample up to ≈ 28 nm for the sample having the highest Fe content.

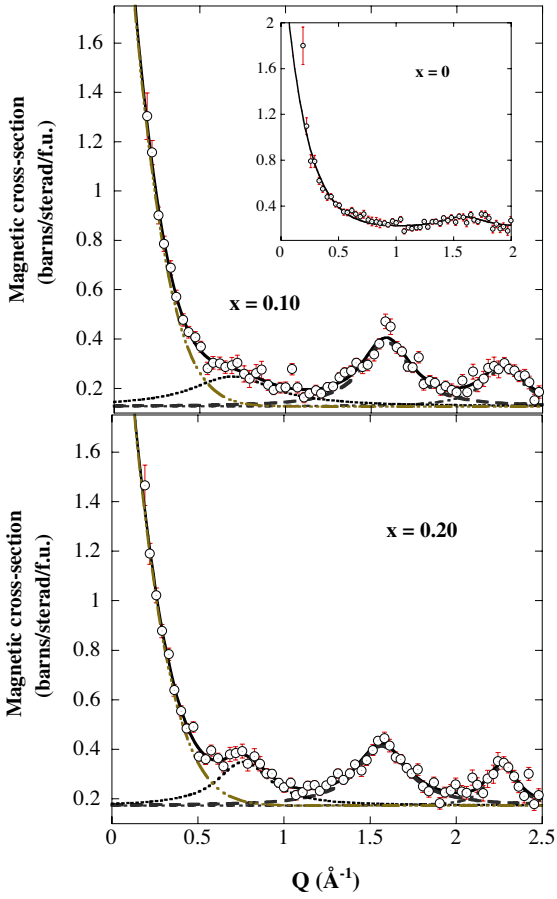

Figure 7. Single-differential magnetic cross-section expressed in units of b/sr/formula unit for compositions $x = 0.10$ (upper) measured at $T = 245$ K and $x = 0.20$, $T = 120$ K (lower) frame. The inset shows the spectrum for the $La_{0.7}Pb_{0.3}MnO_3$ parent compound for $T = 370$ K. Experimental data are depicted by open symbols, and the fitted model consisting of a SANS component (see text) plus two Voigt functions is shown by the solid line. The individual model components are shown by dashed and dash–dot lines.

3.2. Magnetic scattering: polarized neutrons

A set of spectra depicting the purely magnetic cross-section $\frac{d\sigma}{d\Omega}|_m$ for some of the samples and temperatures around the onset of magnetic ordering transition is shown in figure 7.

As can easily be seen from figure 7, Fe-doped samples exhibit, apart from the SANS component considered in the previous section, a set of three diffuse-scattering peaks. The location of the most intense at $Q = 1.58$ Å^{-1} matches that of the lowest structural peak which for $x < 0.2$ gives rise to the (012) magnetic Bragg reflection of the $R\bar{3}m$, $Z = 6$ perovskite structure [20]. The feature appearing at $Q = 2.27$ Å^{-1} also matches the weak overlapping (110) + (104) reflections which again give rise below T_C to identifiable magnetic Bragg reflections for both the parent and Fe content below $x = 0.2$. Notice however that the last composition was found to be devoid of magnetic long-range order down to very low temperatures. In fact, and because of the absence of any strong Bragg contribution or such a

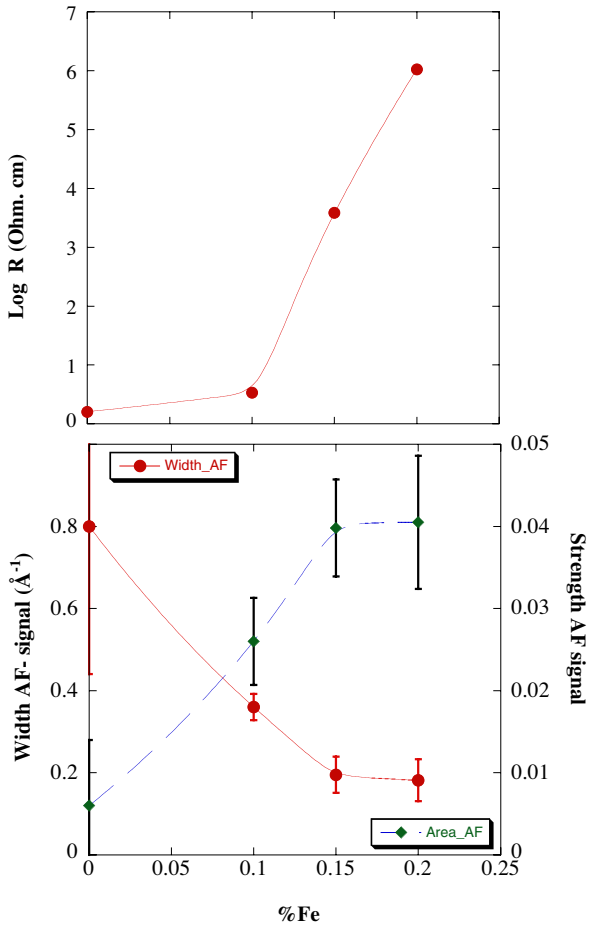

Figure 8. The upper frame shows the concentration dependence of the electrical resistance at $T = 60$ K. The lower frame depicts the dependence upon Fe composition of the linewidth and integrated intensity for the AF signal appearing at $Q \approx 0.8$ Å^{-1}.

composition, the temperature evolution down to 1.5 K of the feature located at $Q = 1.58$ Å^{-1} was recorded. Its intensity was found to exhibit a mild dependence with temperature [23], showing a small drop when crossing T_C from below.

The broad shoulder appearing at the tail of the SANS signal has not been reported in any previous study. Its location at $Q \approx 0.75$ comes close to that corresponding to twice the spacing corresponding to the (012) reflection, which suggests ascribing its origin to an antiferromagnetic (AF) component. Further support for such an assignment is provided by the fact that only a very weak remnant of such a feature is present in the parent $La_{0.7}Pb_{0.3}MnO_3$ sample, as shown by the inset of figure 7. Furthermore, the integrated intensity of such a feature as well as the estimate of its linewidth show a systematic dependence with sample composition as depicted in figure 8. From the linewidth ΔQ of such broad components and account made of finite resolution effects, we derive some estimates of the characteristic sizes of such AF short-range-ordered regions which significantly decrease with increasing Fe content. In real numbers the result yields values that go from $\xi_{AF} = 2\pi/\Delta Q = 17.4$ Å for $x = 0.10$ up to 31.4 Å for

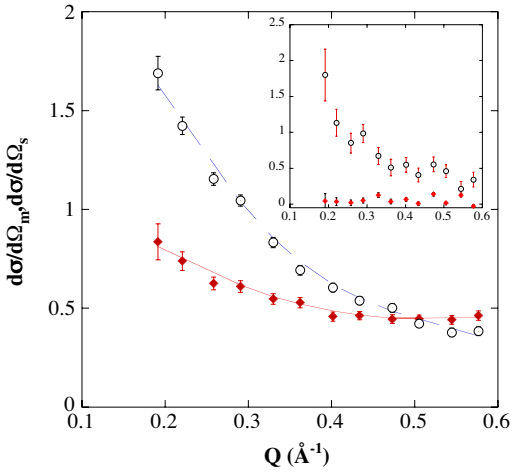

Figure 9. A comparison of the relative strength of the SANS signals of magnetic (circles) and structural (lozenges) origin. Data are plotted on an absolute scale of b/sr/formula -unit and correspond to the sample with $x = 0.15$. The inset shows data for the parent compound.

$x = 0.20$. On the other hand the integrated intensity (strength) of such AF regions also follows a significant dependence with composition, reaching maximal values for $x = 0.15$.

Finally, the complete separation of structural (nuclear), magnetic and spin-incoherent components provided us with a way to check the correctness of the model employed in equation (2) to analyse the low-to-middle-angle data. A graph showing the relative strength of the magnetic and nuclear (structural) SANS signals is shown in figure 9. There we see that within the range of wavevectors reachable by the unpolarized diffraction experiment (i.e. below $Q \approx 0.35$ Å^{-1}) the dominant intensity is of magnetic origin. Moreover, the same structure factors employed in the analysis of the D16 data are shown to fit the polarized neutron data shown in figure 9, where the only adjustable parameter employed were the scale factors A_T and A_m of equation (2). The results depicted in the inset of figure 9 also reveal that the $La_{0.7}Pb_{0.3}MnO_3$ sample shows within this range of momentum-transfers no SANS intensity of structural origin. This particular detail correlates with the larger grain sizes of this sample if compared to the Fe-doped compounds as well as to the significant smaller extent of structural distortions expected for this sample if compared to the Fe-doped compounds.

4. Discussion and conclusions

The parent compound of this series, $La_{0.7}Pb_{0.3}MnO_3$, exhibits significant inhomogeneities which may be described in terms of a model fluid composed of magnetic droplets of radius R_{av} where the nanoscale magnetic structure of such a material once within the FM domain (below 350 K) arises from the interaction of clusters of sizes 21–25 Å that are the main entities mediating the magnetic ordering transition. Increasing Fe doping leads to broadening of the main ordering transition which for $x = 0.2$ spreads over several tens of kelvins and reaches a situation where 3D long-range correlations cease to exist, as attested by the absence of sharp magnetic Bragg reflections. Our results show that apart from changes in ordering temperature as well as spreading the PM $\longrightarrow$ FM transition, Fe doping significantly increases the cluster size with respect to that for the parent compound. In contrast a significantly lower packed structure is found for the Fe-doped compounds. In real numbers, the packing fractions as

calculated from $\eta = \frac{\pi}{6} n d_{\min}^3$ varies from 0.49 for the parent compound, that represents a significantly packed structure to 0.32 for $x = 0.10$. In other words, and in terms of the sketched models, such as that shown in figure 1 of the second reference in [4], the strong enhancement of the CMR effect achieved for the $x = 0.1$ sample with respect to the parent compound is accompanied by the formation of a significantly looser magnetic structure at the nanoscale, where FM regions are separated by the walls of a competing, insulating state. A further increase in Fe doping up to $x = 0.15$ leads to the loss of metallic character as witnessed by the resistance data shown in figure 8 while attaining finite values for the zero-field magnetization below the ordering temperature. Finally, the sample with $x = 0.20$ shows a behaviour more akin to those exhibited by spin glasses than those characteristic of CMR materials.

By polarized neutron diffraction, direct evidence of inhomogeneous regions within $La_{0.7}Pb_{0.3}MnO_3$ within its PM phase is given. Such regions give rise to a magnetic SANS signal which persists down to the lowest explored temperatures, as the unpolarized data demonstrate.

The present data show that the low-temperature FM state gets largely perturbed by Fe doping which gives rise to AF regions which become increasingly important as Fe concentration raises. Data on the diffuse scattering intensity of FM origin involving reflections located where (012) and (110) + (104) magnetic Bragg peaks appear for $x < 0.2$ can be rationalized as arising from short-range-ordered magnetic regions that persist well into the PM phase. Our data, cast in terms of a domain length, show that such a quantity involves distances as given by $2\pi/\Delta Q$ of about 24, 15 and 19 Å for $x = 0.10$, 0.15 and 0.20 respectively for the lowest-order reflection and 36, 40 and 42 Å for the higher-order peak.

A pictorial view of the arrangement of magnetic inhomogeneities is shown in figure 10. There we see that, for low (or no) iron content, macroscopic magnetic phenomena arise from interactions of magnetic particles which lead below T_C to the establishment of magnetic order only within a relatively small region (about 20 nm) within the crystal grains. The characteristic sizes of such magnetically ordered domains drawn as polyhedra in figure 10 are derived on the basis of the measured peak widths of magnetic Bragg peaks. As also sketched in the figure, such domains arise from interactions involving a relatively small number of FM droplets. Up to $x = 0.15$, the spontaneous magnetization arising from interactions between the larger domains yields the finite values for the magnetic moment given above. Above T_C magnetic short-range order at length scales of the order of a few nanometres is preserved as proven by the polarized diffraction experiments. Increasing the Fe doping up to $x = 0.2$ hampers the formation of the larger magnetic domains, and consequently, such a cooperative phenomenon ceases to exist. Ordering within such sample can however be induced by application of external fields as low as 0.5 T [23].

The simplified pictorial description just described shares common ground with the view recently proposed by Hennion *et al* [32, 2, 33]. Our results are thus compatible with a picture where relatively large FM (or hole-poor) clusters separated by distances of the order of about twice the cluster radius achieve spontaneous magnetization as a result of a percolation transition. Entering into a magnetically ordered phase means that a fully ordered state is never achieved, as the presence of diffuse intensity down to the lowest temperature is here witnessed for all our samples.

As regards previous work on closely related issues, the existence of spin clusters in our family of compounds was inferred from low-field ferromagnetic resonance [34]. Also, several previous papers [35–37], report on findings of both AF and FM short-range order within either the PM phase [35] of a two-dimensional $La_{1.2}Sr_{1.8}Mn_2O_7$ CMR perovskite, $Pr_{0.67}Ca_{0.33}MnO_3$ [36] or $La_xCa_{1-x}MnO_3$ [37] at several doping regimes. Data from the latter two are interpreted in terms of microphase-separation where the FM coexists as thin layers within the AFM matrix (i.e. a 'red cabbage') structure [36] or as the result of electronic phase

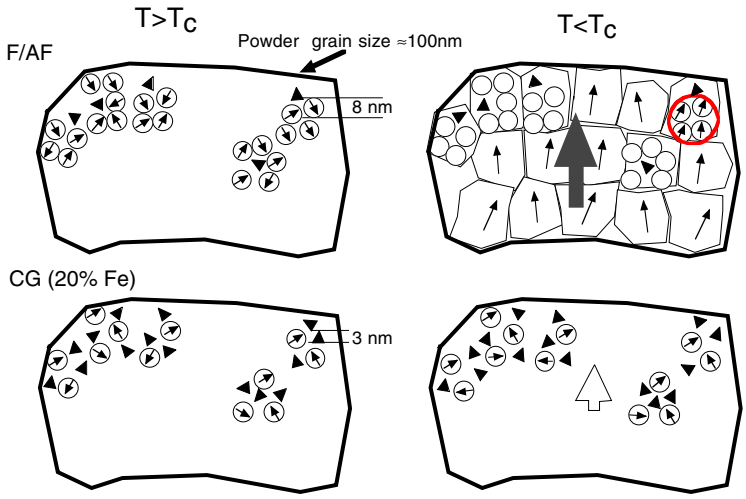

Figure 10. A pictorial view of magnetic ordering phenomena for low (coexisting ferro (F), antiferromagnetic (AF) correlations) and high Fe doping (a cluster glass, CG) contents. The left-hand side displays the magnetic structure as measured by means of polarized neutron diffraction and low-to-middle-angle total diffraction for temperatures above or about the macroscopic ordering transitions signalled by T_C. Open circles depict magnetic short-range-ordered ferromagnetic droplets having characteristic diameters of ≈80 Å. Filled triangles depict AF short-range-ordered regions proved by polarized neutron diffraction. As shown by the frames at the right-hand side, low Fe doping induces ordering within magnetic domains which leads to the appearance of a net macroscopic magnetic moment in the absence of applied field. Higher Fe doping preempts the achievement below T_C of magnetic ordering at length scales beyond those defined by the droplet sizes. Low values for the macroscopic magnetic moment can be achieved under applied fields, as schematically shown by the lower-right-hand frame.

segregation into small FM clusters (10 Å diameter) embedded within the AFM matrix of the undoped compound [37]. Our present data provide some contrasting examples with respect to these previous reports since the same behaviour appears in a truly three-dimensional material as ours. Also, our data show for compositions $x < 0.2$ a well-defined maximum in the SANS intensity at relatively low momentum transfers. Such a finding gives additional support to the adequacy of a model of liquid droplets separated by an average distance $d_{av} = 2\pi/Q_p \approx$ 12.5 nm to describe the magnetic structure. Also, such a result tells us about significant differences between the behaviour of our samples and those of $Pr_{0.67}Ca_{0.33}MnO_3$ [36]. The SANS data for the latter are interpreted as evidences of competing FM and AFM correlations forming infinite two-dimensional sheets on the basis of a Q^{-2} component of the diffraction spectra that dominated the diffraction patterns at the largest momentum-transfers.

Finally, if compared to data reported in [37] which were analysed in a way akin to ours, data for La-doped $CaMnO_3$ [37] show that cluster packing decreases with increasing La doping while ours show that such a trend persists for Fe doping up to $x = 0.1$. Both reports may well be witnessing a common phenomenon since that by Granado *et al* [37] refers to increasing amounts of FM correlations brought forward by La doping within the AFM matrix, while ours concerns the growth of AFM correlations induced by Fe within the FM matrix of the $La_{0.7}Pb_{0.3}MnO_3$ parent compound.

In summary, the present study has served to validate the separation of the cross-section achieved by modelling and also allowed a further characterization of the effects of Fe doping on the structure at the nanoscale. The presence of nanoscale FM and AFM inhomogeneities

that persist well within the PM phase have been unravelled from the separation of the purely magnetic cross-section achieved in the full neutron polarization study.

Acknowledgments

Work supported in part by grant MAT2002-04540-C05-03 (Spain). The authors are grateful to the ILL staff for technical assistance.

References

[1] Tokura Y (ed) 2000 *Colossal Magnetoresistive Oxides* (Amsterdam: Gordon and Breach)
[2] Hennion M and Moussa F 2005 *New J. Phys.* **7** 84
[3] van Tendeloo G, Lebedev O I, Hervieu M and Raveau B 2004 *Rep. Prog. Phys.* **67** 1315
Dagotto E, Hotta T and Moreo A 2001 *Phys. Rep.* **344** 1
[4] Dagotto E 2002 *Nanoscale Phase Separation and Colossal Magnetoresistance* (Berlin: Springer)
Dagotto E 2005 *New J. Phys.* **7** 67
[5] Nagaev E L 2001 *Phys. Rep.* **346** 387
[6] Zener C 1951 *Phys. Rev.* **81** 440
Zener C 1951 *Phys. Rev.* **82** 403
Anderson P W and Hasegawa H 1955 *Phys. Rev.* **100** 675
de Gennes P G 1960 *Phys. Rev.* **118** 141
Kubo K and Ohata N 1972 *J. Phys. Soc. Japan* **33** 21
[7] Milli A J, Littlewood P B and Shraiman B I 1995 *Phys. Rev. Lett.* **74** 5144
[8] Moreo A, Yuunoki S and Dagotto E 1999 *Science* **283** 2034
[9] Khaliullin G and Killian R 2000 *Phys. Rev.* B **61** 3494
Olés A M and Feiner L F 2002 *Phys. Rev.* B **65** 52414
[10] Rodriguez-Carvajal J, Hennion M, Moussa F, Moudden A H, Pinsard L and Revcolevshi A 1998 *Phys. Rev.* B **57** 3189
[11] Hennion M, Moussa F, Rodriguez-Carvajal J, Pinsard L and Revcolevshi A 1998 *Phys. Rev. Lett.* **81** 1957
[12] Searle C W and Wang S T 1969 *Can. J. Phys.* **48** 2023
Leung L K, Morrish A H and Searle C W 1969 *Can. J. Phys.* **47** 2697
Searle C W and Wang S T 1969 *Can. J. Phys.* **47** 2703
[13] Boo C H, Bridges F, Snyder G J and Geballe T H 1996 *Phys. Rev.* B **54** R15606
de Teresa J M *et al* 1997 *Nature* **386** 256
[14] Hwang H Y, Cheong S W, Radaelli P G, Marezio M and Batlogg B 1995 *Phys. Rev. Lett.* **75** 914
Radaelli P G *et al* 1996 *J. Solid State Chem.* **122** 444
[15] Perring T G, Aeppli G, Hayden S M, Carter S A, Remeika J P and Cheong S W 1996 *Phys. Rev. Lett.* **77** 71
[16] Mirabeau I, Hennion M, Casalta H, Andres H, Gudel H U, Irodova A V and Caneschi A 1999 *Phys. Rev. Lett.* **83** 628
[17] Veglio N, Bermejo F J, Gutierrez J, Barandiarán J M, Peña A, Gonzalez M A, Romano P and Mondelli C 2005 *Phys. Rev.* B **71** 212402
[18] Mydosh J A 1993 *Spin Glasses: An Experimental Introduction* (London: Taylor and Francis)
Hicks T J 1995 *Magnetism in Disorder* (Oxford: Clarendon)
[19] Fernández-Barquin L and García-Calderón R 2005 *J. Phys.: Conf. Ser.* **17** 87
[20] Gutiérrez J, Peña A, Barandiarán J M, Hernandez T, Lezama L, Insausti M and Rojo T 2000 *Phys. Rev.* B **61** 9028
[21] Barandiarán J M, Greneche J M, Hernandez T, Plazaola F and Rojo T 2002 *J. Phys.: Condens. Matter* **14** 12563
[22] Shannon R D 1976 *Acta Crystallogr.* A **32** 751
[23] Gutierrez J, Bermejo F J, Barandiarán J M, Cottrell S P, Romano P, Mondelli C, Stewart J R, Fernández Barquin L and Peña A 2006 *Phys. Rev.* B **73** 054433
[24] Ahn K H, Wu X Y, Liu K and Chien C L 1996 *Phys. Rev.* B **54** 15299
[25] Simopoulos A, Pissas M, Kallias G, Devlin E, Moutis N, Panagiopoulos I, Niarchos D and Christides C 1999 *Phys. Rev.* B **59** 1263
[26] Howe M A 1996 *CORRECT (computer code)* NFL Studsvik
[27] See for instance Farrella D F, Ijirib Y, Kellyb C V, Borchersc J A, Rhyned J J, Dinge Y and Majetich S A 2006 *J. Magn. Magn. Mater.* **303** 318
Hellman F, Shapiro A L, Abarra E N, Robinson R A, Hjelm R P, Seeger P A, Rhyne J J and Suzuki J I 1999 *Phys. Rev.* B **59** 1140

Bellouard C, Mirebeau I and Hennion M 1996 *Phys. Rev.* B **56** 5570
Birgeneau R J, Yoshizawa H, Cowley R A, Shirane G and Ikeda H 1983 *Phys. Rev.* B **28** 1438
[28] Lovesey S W 1984 *Theory of Neutron Scattering from Condensed Matter* vol 2 (Oxford: Oxford Science Publications) chapter 13
[29] Kotlarchyk M and Chen S-H 1983 *J. Chem. Phys.* **79** 2461
[30] Schärpf O and Capellman H 1993 *Phys. Status Solidi* a **135** 359
[31] Williams W G 1988 *Polarized Neutrons* (Oxford: Clarendon) chapter 5, p 232
[32] Hennion M, Moussa F, Lehouelleu P, Wang F, Ivanov A, Mukovskii Y M and Shulyatev D 2005 *Phys. Rev. Lett.* **94** 057006
[33] Hendricksen P V, Linderoth S and Lindgård P A 1993 *Phys. Rev.* B **48** 7259
[34] Pissas M and Likodimos V 2005 *J. Phys.: Condens. Matter* **25** 3903
[35] Perring T G, Aeppli G, Moritomo Y and Tokura Y 1997 *Phys. Rev. Lett.* **78** 3197
[36] Simon Ch, Mercone M, Guiblin N, Martin C, Brulet A and André G 2002 *Phys. Rev. Lett.* **89** 207202
[37] Granado E, Ling C D, Neumeier J J, Lynn J W and Argyriou D N 2003 *Phys. Rev.* B **68** 134440